Origin of Enhanced Reducibility/Oxygen Storage Capacity of $Ce_{1-x}Ti_xO_2$ Compared to CeO_2 or TiO_2

Gargi Dutta,[†] Umesh V. Waghmare,[†] Tinku Baidya,[‡] M. S. Hegde,*[,‡] K. R. Priolkar,[§] and P. R. Sarode[§]

Theoretical Sciences Unit, Jawaharlal Nehru Centre for Advanced Scientific Research, Jakkur Campus, Bangalore 560 064, India, Solid State and Structural Chemistry Unit, Indian Institute of Science, Bangalore 560 012, India, and Department of Physics, Goa University, Taleigao Plateau, Goa 403 206, India

Received February 3, 2006. Revised Manuscript Received May 4, 2006

We determine chemical origins of increase in the reducibility of CeO_2 upon Ti substitution using a combination of experiments and first-principles density functional theory calculations. $Ce_{1-x}Ti_xO_2$ ($x = 0.0-0.4$) prepared by a single step solution combustion method crystallizes in a cubic fluorite structure, confirmed by Rietveld profile analysis. $Ce_{1-x}Ti_xO_2$ can be reduced by hydrogen to a larger extent compared to CeO_2 or TiO_2. Temperature programmed reduction of CeO_2, TiO_2, $Ce_{0.75}Ti_{0.25}O_2$ and $Ce_{0.6}Ti_{0.4}O_2$ up to 700 °C in H_2 gave $CeO_{1.96}$, $TiO_{1.92}$, $Ce_{0.75}Ti_{0.25}O_{1.81}$, and $Ce_{0.6}Ti_{0.4}O_{1.73}$, respectively. An extended X-ray absorption fine structure (EXAFS) study of mixed oxides at the Ti K-egde showed that the local coordination of Ti is 4:4, with Ti−O distances of 1.9 and 2.5 Å, respectively, which are also confirmed by our first-principles calculations. Bond valence analysis of the microscopic structure and energetics determined from first principles is used to evaluate the strength of binding of different oxygen atoms and vacancies. We find the presence of strongly and weakly bound oxygens in $Ce_{1-x}Ti_xO_2$, of which the latter are responsible for the higher oxygen storage capacity in the mixed oxides than in pure CeO_2.

1. Introduction

The amount of oxygen that can be released under reducing conditions and can be taken up under oxidizing condition is called the oxygen storage capacity (OSC).[1,2] Temperature programmed reduction (TPR) by H_2 is generally employed to estimate the OSC. The mechanism of the $CeO_2-Ce_2O_3$ transition associated with oxygen vacancy formation was explained on the basis of first-principles calculations as a possible reason behind the high OSC of ceria.[3] Even though ZrO_2 cannot be reduced by CO or H_2, OSC was enhanced in the $Ce_{1-x}Zr_xO_2$ solid solution.[4−6] This means, in the solid solution, Ce can be reduced much more easily compared to pure CeO_2. CeO_2 and $Ce_{1-x}Zr_xO_2$ are essential components of the oxide support in auto-exhaust catalysis, and, therefore, there exist several reports to explain higher OSC in $Ce_{1-x}Zr_xO_2$ compared to CeO_2.[7−11] A common observation is that the X-ray diffraction (XRD) lines of $Ce_{1-x}Zr_xO_2$ are much broader in the solid solution. This is generally attributed to the decrease in size of crystallites, and, therefore, higher OSC was attributed to a larger surface area of $Ce_{1-x}Zr_xO_2$. It is also possible that the local coordination around Zr in $Ce_{1-x}Zr_xO_2$ is different from the ideal eightfold coordination of Ce in CeO_2, which can lead to broadening of X-ray lines. Extended X-ray absorption fine structure (EXAFS) studies have revealed 4 + 4 coordination for Zr in $Ce_{1-x}Zr_xO_2$.[12,13] Recently, we have done first-principles density functional theory (DFT) calculations to show 4 + 4 coordination for both Ce and Zr, and because of this, two kinds of oxygens, strongly and weakly bound to the metal ions, which are generated upon Zr ion substitution in CeO_2.[14] Atomistic and first-principles calculations have been valuable in studies of ceria and its surfaces[15] and interaction with hydrogen.[16] The role of oxygen vacancies on ceria surfaces in the oxidation of carbon monoxide has been studied.[17]

* To whom correspondence should be addressed. E-mail: mshegde@sscu.iisc.ernet.in.
[†] Jawaharlal Nehru Centre for Advanced Scientific Research, Jakkur Campus.
[‡] Indian Institute of Science.
[§] Goa University.

(1) Trovarelli, A. *Comments Inorg. Chem.* **1999**, *20*, 263.
(2) Yao, H. C.; Yao, Y. F. Y. *J. Catal.* **1984**, *86*, 254.
(3) Skorodumova, N. V.; Simak, S. I.; Lundqvist, B. I.; Abrikosov, I. A.; Johansson, B. *Phys. Rev. Lett.* **2002**, *89*, 166601.
(4) Ozawa, M.; Kimura, M.; Isogai, A. *J. Alloys Compd.* **1993**, *193*, 73.
(5) Ranga Rao, G.; Kaspar, J.; Di Monte, R.; Meriani, S.; Graziani, M. *Catal. Lett.* **1994**, *24*, 107.
(6) Fornasiero, P.; Di Monte, R.; Ranga Rao, G.; Kaspar, J.; Meriani, S.; Trovarelli, A.; Graziani, M. *J. Catal.* **1995**, *151*, 168.
(7) Masui, T.; Ozaki, T.; Machida, K.; Adachi, G. *J. Alloys Compd.* **2000**, *303−304*, 49.
(8) Leitenburg, C.; Trovarelli, A.; Llorca, J.; Cavani, F.; Bini, G. *Appl. Catal., A* **1996**, *139*, 161.
(9) Alifanti, M.; Baps, B.; Blangenois, N.; Naud, J.; Grange, P.; Delmon, B. *Chem. Mater.* **2003**, *15*, 395.
(10) Murota, T.; Hasegawa, T.; Aozasa, S.; Matsui, H.; Motoyama, M. *J. Alloys Compd.* **1993**, *193*, 298.
(11) Mamontov, E.; Egami, T.; Brezny, R.; Koranne, M.; Tyagi, S. *J. Phys. Chem. B* **2000**, *104*, 11110.
(12) Vlaic, G.; Fornasiero, P.; Geremia, S.; Kaspar, J.; Graziani, M. *J. Catal.* **1997**, *168*, 386.
(13) Lemaux, S.; Bensaddik, A.; van der Eerden, A. M. J.; Bitter, J. H.; Koningsberger, D. C. *J. Phys. Chem. B* **2001**, *105*, 4810.
(14) Dutta, G.; Waghmare, U. V.; Baidya, T.; Hegde, M. S.; Priolkar, K. R.; Sarode, P. R. *Catal. Lett.* **2006**, *108*, 165.
(15) Sayle, D. C.; Andrada Maicaneanu, S.; Watson, G. W. *J. Am. Chem. Soc.* **2002**, *124*, 11429.
(16) Sohlberg, K.; Pantelides, S. T.; Pennycook, S. J. *J. Am. Chem. Soc.* **2001**, *123*, 6609.
(17) Sayle, T. X. T.; Parker, S. C.; Catlow, C. R. A. *Surf. Sci.* **1994**, *316*, 329.

10.1021/cm060267i CCC: $33.50
Published on Web 06/20/2006

Higher OSC or increased reducibility of CeO_2 in the CeO_2-TiO_2 solid solution has not been studied in detail. Ti^{4+} ions in principle can be substituted for Ce^{4+} ions forming $Ce_{1-x}Ti_xO_2$. Here, both Ce^{4+} and Ti^{4+} ions can be reduced to +3 states, so reducibility of the solid solution or OSC should be higher compared to CeO_2 or TiO_2. The Ti^{4+} ion substitution in CeO_2 has been shown recently.[18] Here we report synthesis of $Ce_{1-x}Ti_xO_2$ by the solution combustion method, H_2/TPR and a first-principles structural study of solid solutions. The theoretically determined structure of $Ce_{1-x}Ti_xO_2$ is compared with the results of EXAFS. We show that the oxygen sublattice is significantly distorted, leading to destabilization of oxide ions in terms of long Ce−O and Ti−O and short Ce−O and Ti−O bonds; the oxide ions with longer bond distances are weakly bound, which can be utilized for CO oxidation.

2. Methods

2.1. Experiment. $Ce_{1-x}Ti_xO_2$ has been prepared by a solution combustion method. Stoichiometric amounts of ceric ammonium nitrate, titanyl nitrate, and glycine were taken in a glass vessel; the salts were dissolved into solution by adding the minimum amount of water. The solution was heated rapidly at 350 °C. At the point of complete water evaporation, the material ignites into a flame reaching a temperature of above 900 °C. After the combustion is complete, the sample cools to 350 °C in about 1 min. The product was a fine powder of $Ce_{1-x}Ti_xO_2$, which was analyzed for all the measurements. Pure TiO_2 (anatase) has been prepared by the combustion of $TiO(NO_3)_2$ with glycine.[19] OSC (hydrogen uptake) was measured by TPR with 5% H_2 in Ar from 30 to 700 °C at a heating rate of 3°/min. The volume of H_2 taken up for reduction is calibrated against that of CuO. The chemical reactions for the formation of CeO_2 and $Ce_{1-x}Ti_xO_2$ can be written as follows:

$$3(NH_4)_2Ce(NO_3)_6 + 8C_2H_5NO_2 = 3CeO_2 + 10N_2 + 16CO_2 + 32H_2O \quad \text{(a)}$$

$$9(1-x)(NH_4)_2Ce(NO_3)_6 + 9xTiO(NO_3)_2 + 10C_2H_5NO_2 + 14(1-x)C_2H_5NO_2 = 9Ce_{1-x}Ti_xO_2 + 20CO_2 + 28(1-x)CO_2 + 14N_2 + 34(1-x)N_2 + 25H_2O + 71(1-x)H_2O \quad \text{(b)}$$

EXAFS was measured at the Ti K and Ce L_3 edges in transmission mode at the EXAFS-1 Beamline at Elettra Synchrotron Source using Si(111) as the monochromator. The incident and transmitted flux was measured using ionization chambers filled with a mixture of N_2 and He in different ratios. For the measurements, absorbers were prepared by sprinkling finely ground powder on scotch tape and stacking about 10 such sheets together. The amount of sample was calculated such that total absorption coefficient (μx) after the edge was around than 2.5. The energy was calibrated with respect to Cu K edge in Cu metal. Data analysis was done using the open source IFEFFIT analysis package developed by Matt Newville at the University of Chicago.

2.2. Theory. Our total energy calculations are based on DFT with a local density approximation (LDA) of the exchange correlation energy of electrons. While the LDA+U type of corrections are known to be important in the reduced form of ceria,[20] we are mainly interested in the atomic structure which is expected to be less sensitive to these corrections. Compounds based on ceria, which involve a mixed valence of cerium, exhibit a large number of competing local minima of electronic total energy. As the energy differences between the states are small, the ground state can be difficult to access.[20] The addition of the U term to the LDA energy functional facilitates access to the physical ground state by enhancing its stability. Physical results, however, were found to be insensitive to the value of the U parameter.[20] In fact, the LDA results have been found to be better than generalized gradient approximation results by Fabris et al.[20] Interaction between valence electrons and ionic cores is treated using first-principles ultrasoft pseudopotentials.[21] Single particle wave functions (density) were represented on a plane wave basis with an energy cutoff of 30 Ry (150 Ry). Semicore states of Ce and Ti are included in the valence. We have not considered spin polarization in our calculation. The orbitals included in the pseudopotentials are Ti 3s, 3p, 4s, and 3d; Ce 5s, 5p, 5d, and 6s; and O 2s and 2p. We use PWSCF[22] implementation of DFT for these calculations. Ti substitution in CeO_2 is treated using periodic supercells of up to eight formula units of CeO_2 with Ce atoms replaced with Ti according to different concentrations of Ti substitution. Internal structure in each case was optimized to minimize the total energy using the Broyden, Fletcher, Goldfarb, and Shanno-based method.[23]

Integrals over the Brillouin zone were sampled on a 4 × 4 × 4 k-point Monkhorst−Pack[24] mesh for pure CeO_2 and $Ce_{0.75}Ti_{0.25}O_2$ which were simulated with a cubic unit cell with four formula units of MO_2 (M = metal ion). For $Ce_{0.875}Ti_{0.125}O_2$, we used a tetragonal supercell (doubled in the *ab* plane, $c/a = 0.71$) with eight formula units, and the Brillouin zone was sampled on a 3 × 3 × 4 Monkhorst−Pack[24] k-point mesh. For pure TiO_2 in the rutile phase, we used a tetragonal unit cell with $c/a = 0.64$ with two formula units, and the Brillouin zone was sampled with a 4 × 4 × 6 Monkhorst−Pack[24] mesh.

Bond lengths determined from the optimized structures are used to calculate valencies of metal ions following the bond valence method.[25] Bond valence *s* is defined as (a) $s = (R/R_0)^{-N}$ (for Ti−O bonds) and (b) $s = \exp[-(R - R_0)/B]$ (for Ce−O bonds), where *R* is the bond length, R_0 is the length of a bond of unit valence, and *N* and *B* are fitted parameters. For Ce−O bonds, $R_0^{LDA} = R_0(a^{LDA}/a^{exp})$. For Ti−O bonds, $R_0^{LDA} = R_0(v^{1/3LDA}/v^{1/3exp})$, where v is the volume of a unit cell. The atomic valence *V* is obtained by summing the bond valencies associated with a particular ion given by $V = \Sigma_i s_i$.

3. Results

XRD patterns of $Ce_{1-x}Ti_xO_2$ (given in Figure 1a for $x = 0.0$, 0.25, and 0.4) show that oxides crystallize in the fluorite structure. On Ti substitution, X-ray line widths become much broader compared to those of pure CeO_2. Lattice parameters of the oxides have been determined, and a decrease in "*a*" for the Ti substituted oxides is observed as expected (see Table 1). The average crystallite size of $Ce_{0.75}Ti_{0.25}O_2$ obtained from Scherrer's formula is 5.5 nm. The structure could be refined using Rietveld profile analysis as shown in

(18) Luo, M.; Chen, J.; Chen, L.; Lu, J.; Feng, Z.; Li, C. *Chem. Mater.* **2001**, *13*, 197.
(19) Nagaveni, K.; Hegde, M. S.; Madras, G. *J. Phys. Chem. B* **2004**, *108*, 20204.
(20) Fabris, S.; de Gironcoli, S.; Baroni, S.; Vicario, G.; Balducci, G. *Phys. Rev. B* **2005**, *71*, 041102(R).
(21) Vanderbilt, D. *Phys. Rev. B* **1990**, *41*, 7892.
(22) Baroni, S.; Dal Corso, A.; de Gironcoli, S.; Giannozzi, P. http://www.pwscf.org.
(23) http://www.library.cornell.edu/nr/bookcpdf/c10−7.pdf.
(24) Monkhorst, H. J.; Pack, J. D. *Phys. Rev. B* **1976**, *13*, 5188.
(25) Brown, I. D. In *Structure and Bonding in Crystals*; O'Keefe, M.; Navrotsky, A., Eds.; Academic Press: New York, 1981; Vol. II.

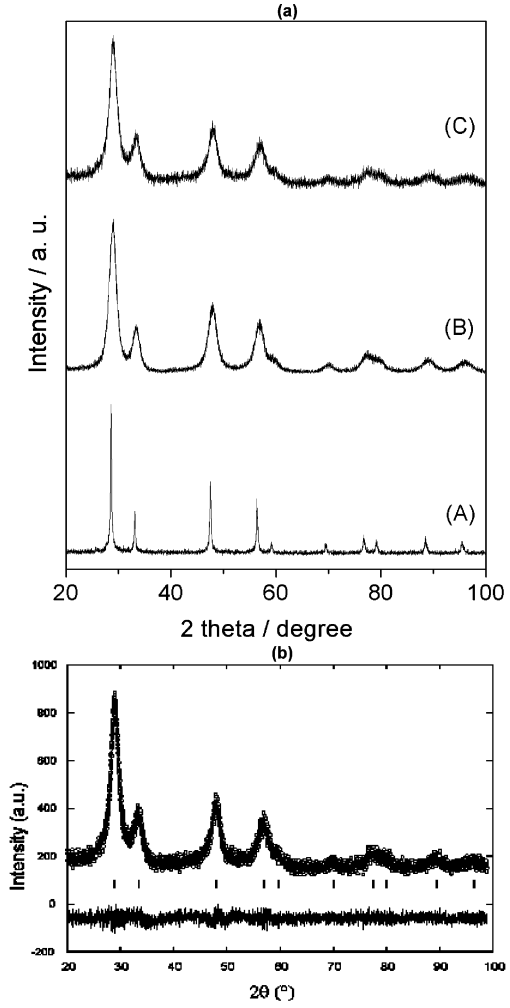

Figure 1. (a) XRD patterns of (A) CeO_2, (B) $Ce_{0.75}Ti_{0.25}O_2$, and (C) $Ce_{0.60}Ti_{0.40}O_2$; (b) Rietveld refined observed (○) and calculated (+) and difference XRD patterns of $Ce_{0.6}Ti_{0.4}O_2$.

Table 1. Lattice Constants, *"a"*, in Å

oxide	calculation	experiment
CeO_2	5.46	5.4131(6)
$Ce_{0.875}Ti_{0.125}O_2$	5.42	5.4011(3)
$Ce_{0.75}Ti_{0.25}O_2$	5.39	5.3950(2)

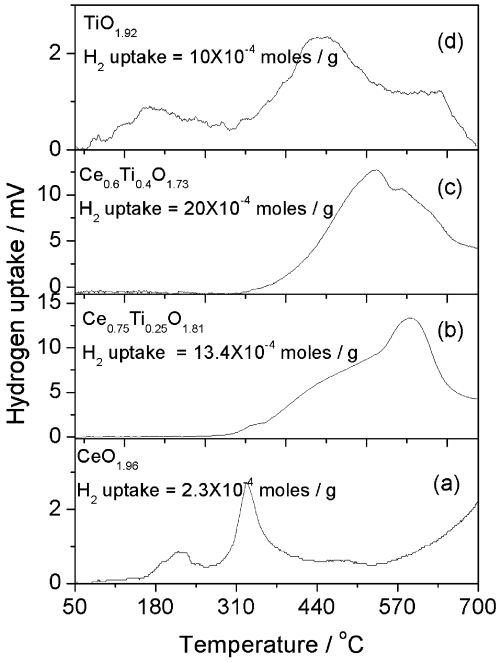

Figure 2. H_2 uptake for CeO_2, TiO_2, and $Ce_{1-x}Ti_xO_2$.

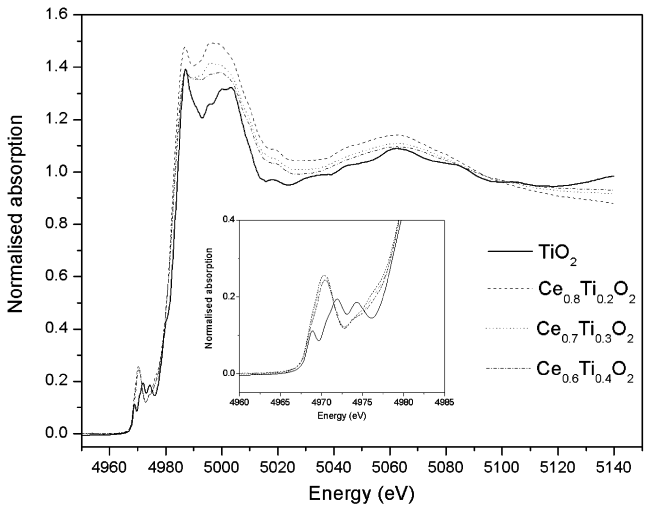

Figure 3. Normalized XANES spectra at the Ti K edge for $Ce_{1-x}Ti_xO_2$.

Figure 1b for $x = 0.4$. As can be seen, the fitting is good. Hydrogen uptake as a function of temperature is shown in Figure 2. Note, the *y* scales are different for different samples. For pure CeO_2, the total H_2 uptake up to 700 °C corresponds to the reduction of CeO_2 to $CeO_{1.96}$, and pure TiO_2 is reduced to $TiO_{1.92}$. With 25 and 40% Ti substitution, the oxides get reduced to $Ce_{0.75}Ti_{0.25}O_{1.81}$ and $Ce_{0.6}Ti_{0.4}O_{1.73}$, respectively. Thus, Ti ion substitution in CeO_2 enhances reducibility by hydrogen. Because of the nanocrystalline nature of the oxides prepared by the solution combustion method, the hydrogen uptake observed here is much higher than that reported by Luo et al.[18]

3.1. EXAFS. Normalized X-ray absorption near edge structure (XANES) spectra at the Ti K edge in $Ce_{1-x}Ti_xO_2$ solid solutions along with that in TiO_2 are presented in Figure 3. Normalization is done by first subtracting the Victoreen instrument background obtained from fitting the pre-edge region (4850 eV to 4950 eV) from the all of the raw spectra and then dividing them by respective average absorption coefficients obtained for the spectral region 5050−5140 eV. It can be seen that the gross XANES features are similar to but slightly broader than those of TiO_2m indicating Ti to be in the 4+ state in the solid solutions. The broadened features indicate the presence of disorder in the solid solutions, which is well-supported by the broad Bragg reflections seen in XRD. The position and the normalized height of the pre-edge peak are known to give a clue of the coordination geometry surrounding the Ti ion.[26] In the case of TiO_2 the pre-edge peak appears at 4971.5 eV and has a normalized height of 0.179, which is in good agreement with the values reported by Farges et al. for 6 coordination geometry. In the case of $Ce_{1-x}Ti_xO_2$ solid solutions, the pre-edge peak appears at 4970.4 eV and has a height of 0.24. Decrease of the pre-edge peak by 1 eV compared to TiO_2 is an indication of a lowering of the coordination around Ti from 6 to a lower value. The values of the height and peak position suggest

(26) Farges, F.; Brown, G. E., Jr.; Rehr, J. J. *Phys. Rev. B* **1997**, *56*, 1809.

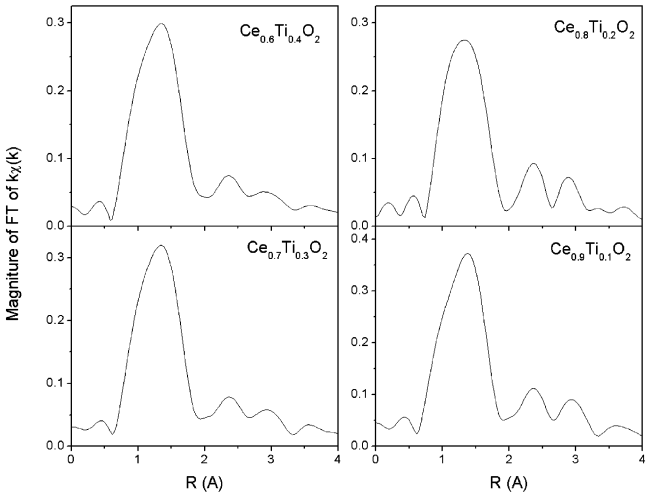

Figure 4. Magnitude of the FT of *k* weighted EXAFS spectra in $Ce_{1-x}Ti_xO_2$.

that Ti has a coordination lower than 5, taking the standard values for model compounds from Farges et al.

The k^2 weighted Fourier transforms (FTs) of the Ti K edge EXAFS in $Ce_{1-x}Ti_xO_2$ for $x = 0.1$, 0.2, 0.3, and 0.4 were examined. The weighted EXAFS data in the *k* range from 2 $Å^{-1}$ to 10 $Å^{-1}$ were transformed to *R* space (see Figure 4). The resulting magnitude of FT exhibited a strong peak at about 1.9 Å corresponding to Ti−O correlations. The peaks in the range from 3 to 4 Å observed are ascribed to Ti−Ti-(Ce) correlations. Because the Ti^{4+} ion is too small to be accommodated for in 8 coordination as for Ce^{4+} in pure CeO_2, oxygen around the Ti ion is distorted, and with one Ti−O distance, the fitting is too poor. EXAFS data were essentially fitted with correlations obtained for the CeO_2 type fluorite structure using FEFF6. However, some essential modifications in the pure CeO_2 structure were considered. First, it was assumed that the entire Ti substitutes for Ce randomly, and, therefore, 12 neighbors in the second shell around Ti ion were distributed as per ratio the of Ce to Ti. Second, to fit the first peak, three oxygen coordinations around Ti were considered, namely, 6+2, 4+4, and 4+2+2, such that total number of oxygen ions surrounding Ti equals eight. In Figure 5 the fitting in the back-transformed *k* space with three distributions is shown for $Ce_{0.6}Ti_{0.4}O_2$. As can be seen, 6+2 coordination does not give a good fit. 4+4 and 4+2+2 coordinations around Ti give good fits, and given the resolution ΔR in *R* space, it is rather impossible to choose any one from among them. The fittings in the back-transformed *k* space for different compositions for 4 + 4 coordination are given in Figure 6. The values of bond lengths and Debye−Waller terms are presented in Table 2. For all the solid solutions studied, it can be seen that the σ^2 values for the second shell are quite large. The results clearly demonstrate that first coordination of Ti^{4+} ions is 4 at a Ti−O distance of 1.9 Å. The other four oxygens are distributed between 2.4 and 2.6 Å. Thus, four oxygens out of eight move closer to the Ti ion at 1.9 Å, and four oxygens move away to longer distances of ∼2.5 Å in 4+4 coordination and 2.4−2.6 Å in 4+2+2 coordination. It is important to note that Ti−O distances at ∼2.5 Å are much longer than the average Ce−O distance of 2.36 Å in CeO_2. Further, Ti−Ti correlation

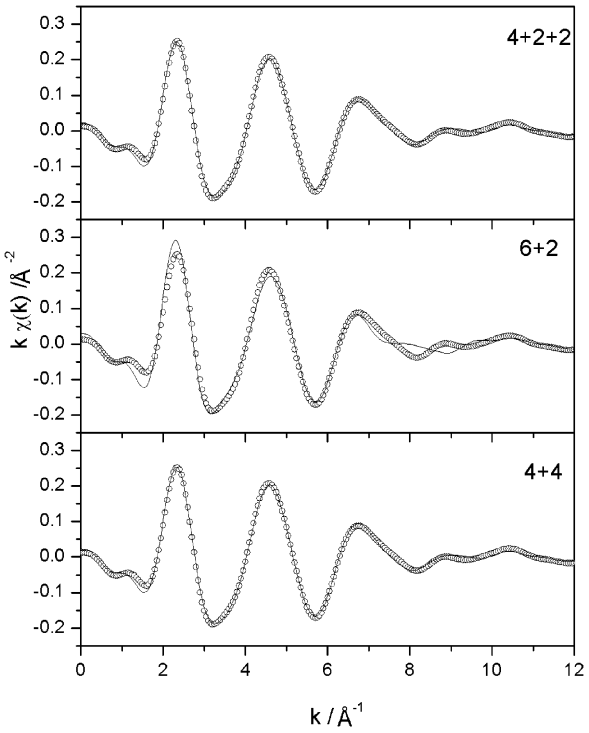

Figure 5. Back transformed EXAFS spectra (circles) at the Ti K edge for $Ce_{0.6}Ti_{0.4}O_2$ along with fits for 4 + 4, 6 + 2, and 4 + 2 + 2 coordinations (solid line).

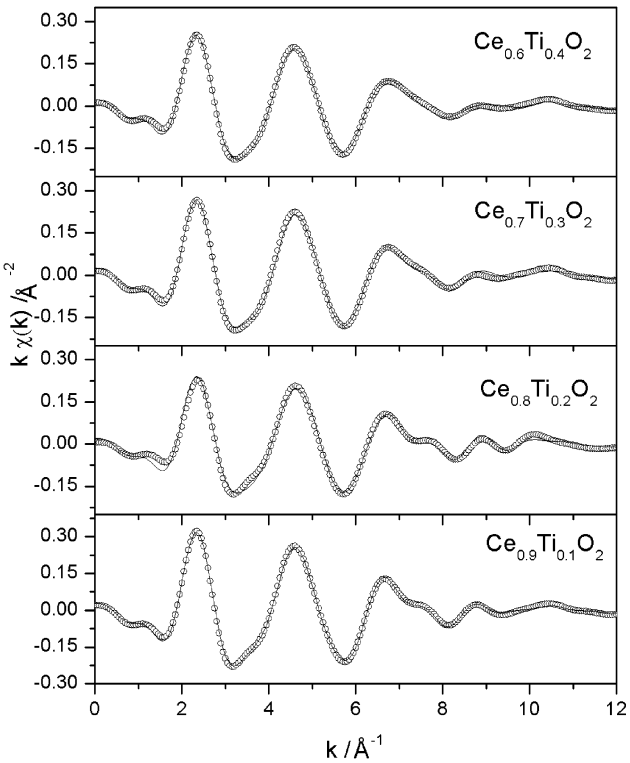

Figure 6. Back transformed EXAFS spectra at the Ti K edge (circles) along with respective fits (solid lines) to 4 + 4 coordination for $Ce_{1-x}Ti_xO_2$.

at 3.0 Å and Ti−Ce correlation at ∼3.5 Å are unique distances.

To gain insight on the effect of Ti substitution on Ce coordination, EXAFS spectra at the Ce L_3 edge were also analyzed. The procedure adapted to fit the EXAFS data was the same as earlier. In this case, however, both the 6 + 2 and 4 + 4 models gave satisfactory fits. This would mean

Table 2. Local Coordination in $Ce_{1-x}Ti_xO_2$ Determined from Ti K edge EXAFS[a]

sample	coordination shell	C.N.	*R*	σ^2
$Ce_{0.6}Ti_{0.4}O_2$	Ti−O	4	1.899 ± 0.003	0.007 ± 0.001
		4	2.466 ± 0.008	0.020 ± 0.002
		4	1.899 ± 0.003	0.007 ± 0.001
		2	2.39 ± 0.01	0.016 ± 0.003
		2	2.53 ± 0.01	0.013 ± 0.003
		6	1.908 ± 0.008	0.016 ± 0.002
		2	2.43 ± 0.03	0.004 ± 0.004
	Ti−Ti	5	3.009 ± 0.014	0.025 ± 0.003
	Ti−Ce	7	3.528 ± 0.020	0.041 ± 0.005
$Ce_{0.7}Ti_{0.3}O_2$	Ti−O	4	1.895 ± 0.004	0.006 ± 0.001
		4	2.467 ± 0.015	0.028 ± 0.004
		4	1.898 ± 0.003	0.006 ± 0.001
		2	2.36 ± 0.03	0.034 ± 0.006
		2	2.52 ± 0.01	0.012 ± 0.003
		6	1.907 ± 0.008	0.016 ± 0.002
		2	2.43 ± 0.02	0.005 ± 0.004
	Ti−Ti	3.5	3.025 ± 0.019	0.025 ± 0.004
	Ti−Ce	8.5	3.55 ± 0.020	0.041 ± 0.005
$Ce_{0.8}Ti_{0.2}O_2$	Ti−O	4	1.901 ± 0.005	0.007 ± 0.001
		4	2.451 ± 0.015	0.015 ± 0.004
		4	1.899 ± 0.003	0.007 ± 0.001
		2	2.39 ± 0.01	0.016 ± 0.003
		2	2.53 ± 0.01	0.013 ± 0.003
		6	1.907 ± 0.009	0.016 ± 0.002
		2	2.42 ± 0.02	0.005 ± 0.004
	Ti−Ti	2.5	3.07 ± 0.02	0.015 ± 0.004
	Ti−Ce	9.5	3.47 ± 0.030	0.047 ± 0.008
$Ce_{0.9}Ti_{0.1}O_2$	Ti−O	4	1.898 ± 0.003	0.005 ± 0.001
		4	2.508 ± 0.011	0.022 ± 0.003
		4	1.901 ± 0.003	0.005 ± 0.001
		2	2.412 ± 0.009	0.006 ± 0.002
		2	2.632 ± 0.015	0.012 ± 0.003
		6	1.905 ± 0.005	0.011 ± 0.001
		2	2.43 ± 0.02	0.006 ± 0.004
	Ti−Ti	1.2	3.017 ± 0.016	0.007 ± 0.004
	Ti−Ce	10.8	3.499 ± 0.019	0.030 ± 0.004

[a] C.N.: coordination number was kept fixed in all the fitting iterations. Bond distance *R* in Å.

that, in the fluorite structure, the substitution of Ti affects the coordination around it as well as Ce. In CeO_2, the Ce−O bond length is obtained at 2.36 Å, but in $Ce_{1-x}Ti_xO_2$, Ce−O bond distances are obtained at 2.30 and 2.42 Å in 4 + 4 coordination. Thus, distortion is more around the Ti ion (1.9 and 2.5 Å) than around the Ce ion. In Table 3 the structural details for the Ce L_3 EXAFS are given, and the FT of the EXAFS data along with fittings to the two representative compounds $x = 0.1$ and $x = 0.4$ are shown in Figure 7. It is important to note that the Ce−Ti distance from the Ce L_3 edge agrees well with the Ti−Ce distance from the Ti K edge study. Thus, the EXAFS study clearly shows two kinds of coordination for Ti as well as Ce; 4 + 4 oxygen coordination around the metal ions is observed for the solid solutions compared to the 8 coordination in pure CeO_2.

3.2. DFT Calculations. The lattice constants determined from first-principles calculations are within the typical DFT errors with respect to their experimental values (see Table 1). The Ce_3TiO_8 cell corresponding to a $Ce_{0.75}Ti_{0.25}O_2$ composition is taken, and because there is only one Ti in this cell, the Ti−Ti near-neighbor distance is not obtained. The Ce−Ce distance obtained is 3.81 Å, which agrees well with the Ce L_3 edge EXAFS study. Total coordination of Ce is 12. Figure 8 shows the coordination around the cations in the optimized structure of $Ce_{0.75}Ti_{0.25}O_2$, in which oxygens O1, O3, O6, and O8 form short Ti−O bonds, while oxygens O2, O4, O5, and O7 form long Ti−O bonds. Four of the eight nearest-neighbor oxygen atoms come closer to the Ti atom, resulting in a coordination of four. O3 forms a short bond with Ti and a long bond with Ce, while O7 forms a long bond with Ti and a short bond with Ce. Hence, those oxygens which move away from the Ti ion move toward the Ce ion and vice versa. From our theoretical calculations, Ti as well as Ce has 4 + 4 coordination of oxygens around the metal ion. The Ti−O distances are 1.85 and 2.76 Å for $Ce_{0.75}Ti_{0.25}O_2$ and 1.87 and 2.71 Å for $Ce_{0.875}Ti_{0.125}O_2$, which are close to the values obtained from EXAFS analysis. The Ce−O distances of 2.22 and 2.53 Å for $Ce_{0.75}Ti_{0.25}O_2$ are close to the EXAFS results. For $Ce_{0.875}Ti_{0.125}O_2$, the average short Ce−O distance is 2.25 Å and the average long Ce−O distance is 2.47 Å, which are also in good agreement with the experimental values obtained from EXAFS.

Table 3. Local Coordination in $Ce_{1-x}Ti_xO_2$ Determined from Ce L_3 Edge EXAFS[a]

sample	coordination shell	C.N.	*R*	σ^2
$Ce_{0.6}Ti_{0.4}O_2$	Ce−O	4	2.305 ± 0.006	0.007 ± 0.001
		4	2.417 ± 0.023	0.042 ± 0.006
		6	2.303 ± 0.006	0.010 ± 0.002
		2	2.574 ± 0.041	0.020 ± 0.011
	Ce−Ce	7	3.861 ± 0.019	0.014 ± 0.003
	Ce−Ti	5	3.609 ± 0.020	0.033 ± 0.011
	Ce−O	24	4.480 ± 0.013	0.021 ± 0.003
$Ce_{0.9}Ti_{0.1}O_2$	Ce−O	4	2.302 ± 0.004	0.004 ± 0.001
		4	2.425 ± 0.011	0.034 ± 0.005
		6	2.305 ± 0.005	0.007 ± 0.001
		2	2.559 ± 0.036	0.020 ± 0.009
	Ce−Ce	11	3.864 ± 0.009	0.010 ± 0.002
	Ce−Ti	1	3.588 ± 0.104	0.030 ± 0.027
	Ce−O	24	4.492 ± 0.009	0.014 ± 0.002

[a] C.N.: coordination number was kept fixed in all the fitting iterations. Bond distance *R* in Å.

With access to local structural details, we carried out bond valence analysis to uncover the cause for the enhanced observed reducibility/OSC. The parameters used in the bond valence calculation[25] are given in Table 4. For pure CeO_2, the average valency of Ce is 3.97, and that of an oxygen is 1.99. On Ti substitution as given in Table 5, the weakly bonded oxygens have valencies (1.62−1.73), which are lower than that in pure CeO_2, while the stronger ones have higher valencies. The Ti valencies in $Ce_{0.75}Ti_{0.25}O_2$ and $Ce_{0.875}Ti_{0.125}O_2$ are 3.65 and 3.54, respectively. The average Ce valencies in $Ce_{0.75}Ti_{0.25}O_2$ and $Ce_{0.875}Ti_{0.125}O_2$ are 4.21 and 4.24, respectively. The presence of reduced ions in mixed oxides is responsible for formation of long and short bonds, which in turn changes the coordination around the cations, leading to the formation of weak oxygens.

Distribution of cation to oxygen distances given in Figure 9a shows the presence of a single Ce−O bond length in pure

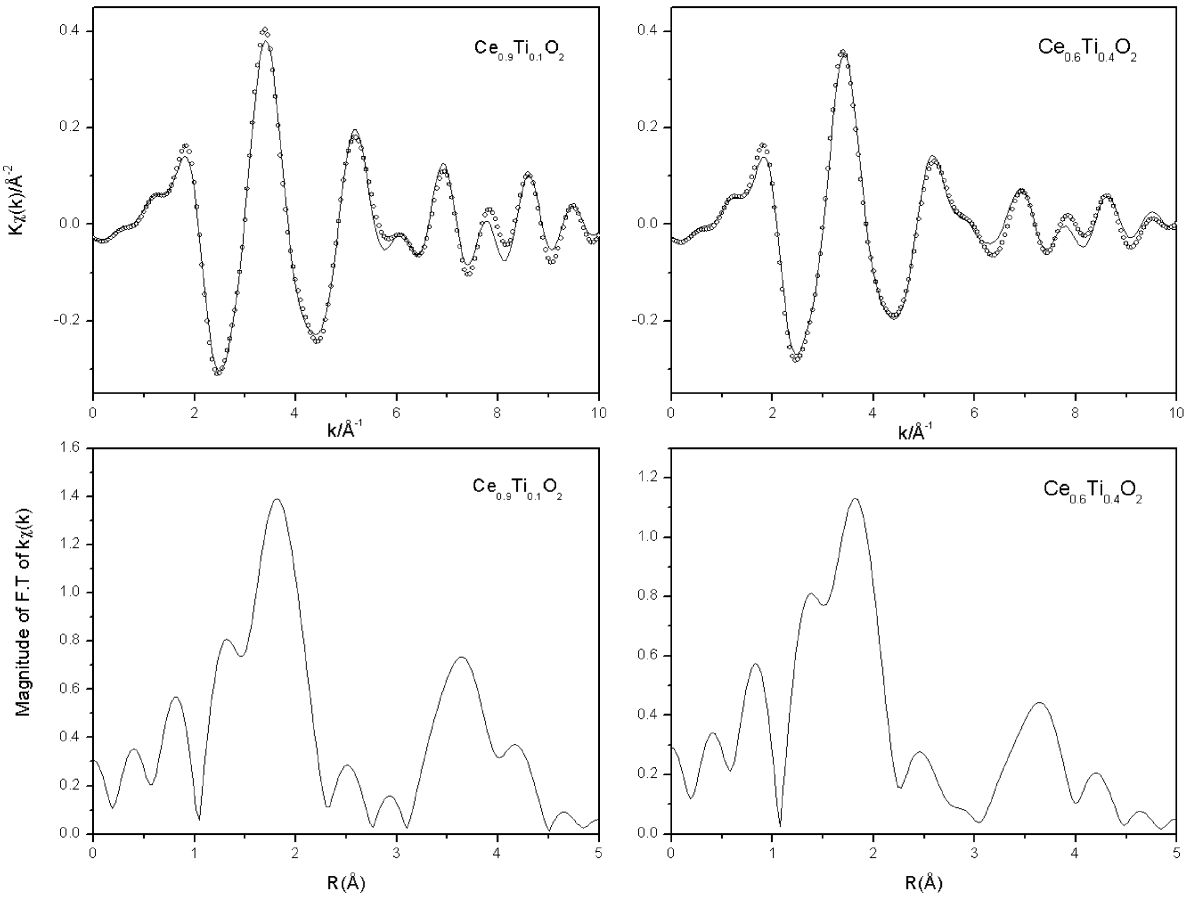

Figure 7. Magnitude of FT and corresponding back transforms of the CeL_3 edge EXAFS in $Ce_{0.9}Ti_{0.1}O_2$ and $Ce_{0.6}Ti_{0.4}O_2$. The solid lines indicate fits to the data.

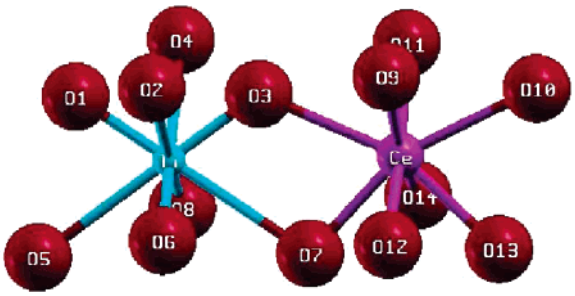

Figure 8. $Ce_{0.75}Ti_{0.25}O_2$, showing the coordination around Ti and Ce ions.

Table 4. Parameters Used in Bond Valence Calculation[a]

type of bond	R_0	R_0^{LDA}	constant
Ce−O	2.12	2.14	$B = 0.33$
Ti−O	1.81	1.78	$N = 5.20$

[a] All distances are given in Å.

CeO_2 at 2.36 Å. On Ti substitution, the bond lengths can be divided into two categories, short and long, where the short category falls below 2.36 Å and the long category falls above 2.36 Å. In $Ce_{0.875}Ti_{0.125}O_2$, three types of short and three types of long bonds are found. In $Ce_{0.75}Ti_{0.25}O_2$, two types of short and two types of long bonds are found. Table 6 shows the average values of bond lengths in Ti substituted CeO_2. The long bonds are weaker, and the short bonds are stronger, hence, the availability of longer bonds in Ti doped CeO_2 leads to higher OSC than pure CeO_2. Such a distortion of the oxygen sublattice is responsible for the broadening of Bragg reflections in XRD. Thus, from the bond valence

Table 5. Calculation of Oxygen Valencies in Ceria−Titania[a]

mixed oxide	oxygen valency	bonds made by oxygen
$Ce_{0.75}Ti_{0.25}O_2$	2.37	3 Ce−O short bonds, 1 Ti−O long bond
	1.70	3 Ce−O long bonds, 1 Ti−O short bond
$Ce_{0.75}Ti_{0.25}O_{1.75}$	2.53	3 Ce−O short bonds, 1 Ti−O long bond
	2.31	3 Ce−O short bonds, 1 Ti−O long bond
	1.73	3 Ce−O long bonds, 1 Ti−O short bond
$Ce_{0.875}Ti_{0.125}O_2$	2.41	3 Ce−O short bonds, 1 Ti−O long bond
	2.21	3 Ce−O long bonds, 1 Ce−O short bond
	2.06	3 Ce−O short bonds, 1 Ce−O long bond
	1.62	3 Ce−O long bonds, 1 Ti−O short bond

[a] The oxygens having three Ce−O long bonds and one Ti−O short bond form the weaker catagory.

analysis, two types of oxygens can be identified: type 1 (strong) and type 2 (weak).

The total cohesive energy E can be expressed in terms of bond energy $\epsilon(b)$: $\int \epsilon(b)\, D(b)\, db = E$, $D(b)$ being the distribution of bond lengths or the bond length density. To determine energies of short and long bonds in $Ce_{1-x}Ti_xO_2$, we assume the following simple relation: $E_{type1}/E_{type2} = \mathrm{av}(s_{type1})/\mathrm{av}(s_{type2})$, where $\mathrm{av}(s)$ is the average bond valence of a type of bond. According to the bond valence theory, valence of an atom is a measure of its involvement in bonding.[25] As the valence of an atom is the sum of its individual bond valences, it is reasonable to assume that the higher the bond valence, the stronger the bond and vice versa.

The relative bonding energies in $Ce_{0.75}Ti_{0.25}O_2$ given in Table 7 show that Ce−O (long), Ti−O (long), and Ti−O (short) bonds are weaker than the pure Ce−O bond. We have

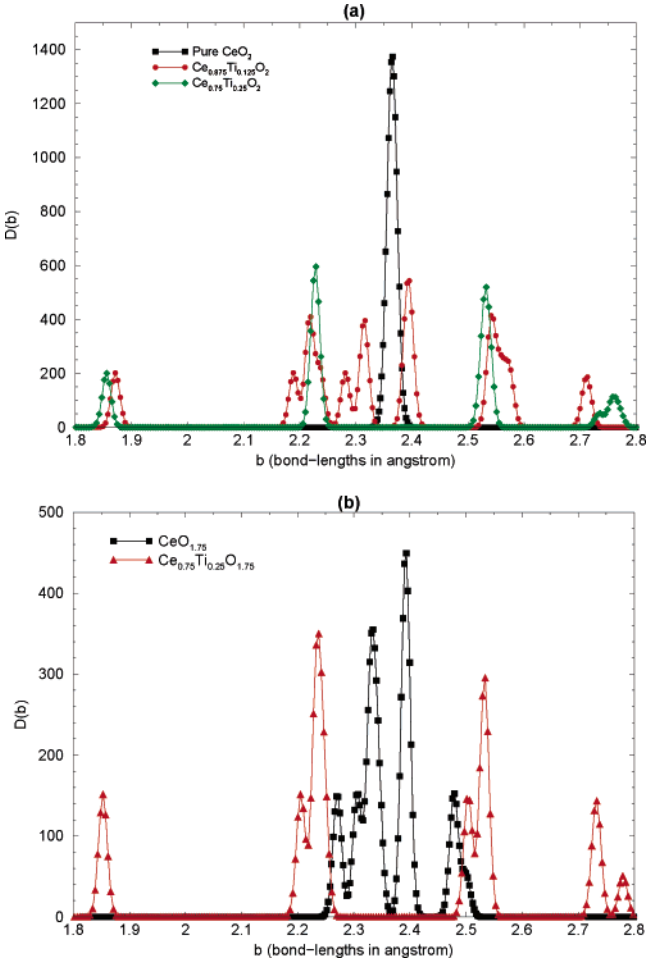

Figure 9. Distribution of cation−oxygen bond lengths in (a) CeO_2-TiO_2 and (b) vacancy-introduced CeO_2-TiO_2.

Table 6. Bond Lengths in Ceria−Titania

oxide	bond lengths
pure CeO_2	2.36 (Ce−O)
$CeO_{1.75}$	2.27, 2.33, 2.39, 2.48 (Ce−O)
$Ce_{0.875}Ti_{0.125}O_2$	(2.19, 2.22), (2.28, 2.31), 2.39, 2.54 (Ce−O)
	1.87, 2.71 (Ti−O)
$Ce_{0.75}Ti_{0.25}O_2$	2.22, 2.53 (Ce−O)
	1.85, 2.76 (Ti−O)
$Ce_{0.75}Ti_{0.25}O_{1.75}$	(2.20, 2.24), (2.50, 2.53) (Ce−O)
	1.85, 2.73, 2.78 (Ti−O)

[a] All distances in Å. The bond lengths within brackets correspond to peaks which are close together in the bond length distribution plots (Figure 9).

Table 7. Strength of Bonds in $Ce_{0.75}Ti_{0.25}O_2$: Relative Difference in Bonding Energy with Respect to the Ce−O Bond in Pure CeO_2[a]

type of bond	relative difference in bond strengths (%)
Ce−O (long)	−43.60
Ce−O (short)	+43.31
Ti−O (long)	−91.23
Ti−O (short)	−31.65
Ce−O	0.0

[a] The "−" denotes a weaker bond, and "+" denotes a stronger bond.

showed the percent difference in the bonding energies with respect to pure Ce−O bond because their absolute values are typically overestimated in LDA calculations.

The binding energy of different types of oxygens is obtained by summing up of individual bond energies. The relative binding energy of oxygens in Ti substituted CeO_2 is given in Table 8. For pure CeO_2, we have a single type of oxygen, in which each oxygen forms four bonds with Ce. For $Ce_{0.75}Ti_{0.25}O_2$, the binding energy of an oxygen with three Ce−O short bonds and one Ti−O long bond is given by type 1 and has a binding energy more than that of an oxygen in pure CeO_2. Type 2 has oxygen that has three Ce−O long bonds and one Ti−O short bond and is more weakly bound than an oxygen in pure CeO_2. Our analysis of bond strengths is consistent with the result that the cohesive energy of $Ce_{0.75}Ti_{0.25}O_2$ is 15.51% smaller than that of pure CeO_2.

Table 8. Relative Binding Energy (BE) of Different Types of Oxygens in $Ce_{0.75}Ti_{0.25}O_2$ with Respect to an Oxygen in Pure CeO_2, where Each Oxygen Forms Four Bonds with Cations[a]

oxide	type of oxygen	% change of BE	no. of each type
pure CeO_2	single type	0.00	8
$Ce_{0.75}Ti_{0.25}O_2$	type 1 (strong)	+9.67	4
	type 2 (weak)	−40.62	4

[a] The "−" denotes a weak oxygen, and "+" denotes a strong oxygen.

To probe further the OSC of mixed oxides, we have analyzed effects of oxygen vacancies introduced in the tetrahedral position. $Ce_{0.75}Ti_{0.25}O_{1.75}$ is a structure with 12.5% oxygen vacancy. The total energy obtained from our calculations for the single "O" atom is −425.87 eV, while that of half of a molecular oxygen is −430.54 eV. Because $Ce_{0.75}Ti_{0.25}O_{1.75}$ has one oxygen vacancy, we compare its cohesive energy with that of $Ce_{0.75}Ti_{0.25}O_2$ by keeping the same number of atoms in each case and, hence, adding one oxygen with energy of −425.87 eV to $Ce_{0.75}Ti_{0.25}O_{1.75}$. The oxygen added is an atomic oxygen. We have not considered spins in our calculation. Our calculated cohesive energies of $Ce_{0.75}Ti_{0.25}O_2$ and ($Ce_{0.75}Ti_{0.25}O_{1.75}$ + an oxygen) suggest that it will cost an energy of 11.55 eV to create an oxygen vacancy. Similarly, the difference in cohesive energies of CeO_2 and ($CeO_{1.75}$ + an oxygen) is 11.83 eV. If one of the oxide ions is removed from the tetrahedral position to the octahedral vacant position, on relaxing the structure the oxygen moves back to the tetrahedral position resulting in the original structure without vacancy and having the same energy. Thus, it rules out the possibility for an oxygen atom to occupy the octahedral site in the bulk form of these oxides. Our calculations with oxygen vacancy in ceria−titania show that the presence of an oxygen vacancy makes the structure weakly bound and increases the number of weak oxygens, contributing to higher OSC.

Figure 9b shows the presence of both short and long bonds in vacancy-introduced ceria as in $CeO_{1.75}$ compared to the single bond length of 2.36 Å in pure CeO_2. Presence of longer bonds compared to CeO_2 shows the availability of weaker oxygens in $CeO_{2-\delta}$. This could also be a reason for the enhanced reducibility of $Ce_{1-x}Ti_xO_2$; initial removal of oxide ions at lower temperature enhances further removal of oxygen. The broad H_2 uptake curve indeed supports this calculation.

Hence, presence of oxygen vacancies is an important factor which affects the OSC in mixed oxides (see Table 6 for bond lengths in vacancy introduced mixed oxides). The values of the oxygen valencies for $Ce_{0.75}Ti_{0.25}O_{1.75}$ are given in Table 5. In each case, the numbers of strong and weak oxygens

are four and three, respectively. Hence, it shows that the position of the tetrahedral vacancy was the site of a weakly bound oxygen.

4. Conclusions

In this paper the higher OSC of the Ti doped CeO_2 solid solution is probed by EXAFS and DFT calculations. The EXAFS study of $Ce_{1-x}Ti_xO_2$ shows that oxygen coordination around Ti is distorted, resulting in 4 + 4 distribution such that 4 oxygens come close to Ti at 1.9 Å while the other 4 move away at 2.5 Å. The structures determined from our first-principles calculations agree well with the EXAFS results. We find that the presence of short and long bonds results in two types of oxygens: strongly and weakly bound. The stronger ones have a valency greater than 2.0, and the weaker ones have a valency less than 2.0. Using the valencies of cations and oxygens calculated by the bond valence method and binding energies, we determined the weakly bound oxygens responsible for higher OSC in the mixed oxides.

Acknowledgment. The authors thank the central computing facility at JNCASR for use of computational resources, U.V.W. acknowledges a DuPont Young Faculty Grant, and G.D. thanks UGC for research fellowship. K.R.P. and P.R.S. acknowledge the financial assistance from Department of Science and Technology, Govt. of India, and Elettra-ICTP under Indo-Italian POC for the Proposal No. 2004676 and thank Prof. G. Vlaic and Dr. Luca Olivi for help and useful discussions.

CM060267I